applied sciences

MDPI

Article

A New Flow Control Method of Slat-Grid Channel-Coupled Configuration on High-Lift Device

Jingyi Yu and Baigang Mi *

School of Aeronautics, Northwestern Polytechnical University, Xi'an 710072, China
* Correspondence: mibaigang@163.com

Abstract: A slot formed between the slat and the main wing of the 2D high-lift device is used to accelerate the convergence of the flow to the upper surface of the main wing to improve the flow field quality. In order to further enhance flow characteristics, this paper proposes a design method for multi-channel leading-edge slats based on grid flow channels. On the one hand, a specific shape of a shrinking expansion tube is formed to improve the lift characteristics of the leading slat. On the other hand, the newly formed slot plays a similar role to that of the jet stream, delaying the separation on the upper surface of the main wing, making the separation point move back and helping to improve the lift characteristics of the main wing. The optimization of coupled slat-grid channel configuration is developed by using the DOE algorithm. The geometric parameters, such as coordinates and curve slope, are considered as design variables, and the maximum lift–drag ratio is taken as the optimization objective required to obtain the optimal configuration. The simulation and optimization results show that the lift coefficient increases by 3.3%, the drag coefficient decreases by 12.7%, and the lift–drag ratio increases by 18.4% of the optimal configuration compared with the original airfoil at an angle of attack of 16.3°.

Keywords: grid-fin; multi-element configuration; flow control; aerodynamic optimization; DOE optimization algorithm

Citation: Yu, J.; Mi, B. A New Flow Control Method of Slat-Grid Channel-Coupled Configuration on High-Lift Device. *Appl. Sci.* **2023**, *13*, 3488. https://doi.org/10.3390/app13063488

Academic Editors: Francesca Scargiali, Gabriel Bugeda Castelltort and Josep Maria Bergadà

Received: 30 December 2022
Revised: 22 February 2023
Accepted: 6 March 2023
Published: 9 March 2023

1. Introduction

For the commonly used three-stage high-lift device, the flow characteristic is that the leading slat and trailing-edge flaps work together to improve the lift–drag characteristics of the entire airfoil. Van Dam [1] reviewed the recent developments in aerodynamic design and analysis methods for multi-element high-lift systems in transport airplanes, including necessity, the major design objectives, and constraints. For the commonly used three-stage high-lift device, the flow characteristic is that the leading slat and trailing-edge flaps work together to improve the lift–drag characteristics of the entire airfoil. In 1970, A. Smith [2] analyzed the aerodynamic principle of the multi-element configuration, and believed that it was affected by the slat effect, circulation effect, off-the-surface pressure recovery, and boundary layer effect of each wing segment. It is well recognized that the usual function of the slot is that of a boundary layer control device, permitting highly adverse upper-surface pressure gradients to be sustained without incurring severe separation. There appear to be five primary effects of gaps, and here we speak of properly designed aerodynamic slots. According to the current classical active and passive flow control theories, the mechanism of the three-segment high-lift device can be classified into the passive control method. The passive flow control technology does not add energy to the flow, but changes the flow boundary or pressure gradient through some methods to control the flow, such as optimizing the geometric parameters of the airfoil, adding or combining flow control devices, and through fixed-point displacement or deformation under specific working conditions. Compared with active flow control technology [3], it is widely valued for its advantages of simple structure, lack of additional energy consumption or lower energy consumption, and low cost. For the three-stage high-lift device, the leading-edge slat can accelerate the airflow through the slots formed with the main wing, forming a similar effect to the jet flow, which can favorably disturb the airflow of the main wing and improve its wind resistance. However, the practical application of this three-element high-lift device has many limitations. For example, the aircraft is significantly affected by the ground effect during takeoff and landing. For the high-lift device, the flaps are deflected closer to the ground [4], meaning that the impact is greater. For amphibious aircraft [5,6], flap failure may even occur due to body splash. In order to further improve the aerodynamic characteristics and practical value of the high-lift device, slats are the preferred component for optimization and improvement.

The basic principle of slat lift enhancement is that there is a gap between the slat and the leading-edge surface of the main wing. Specifically, the velocity of the airflow on the lower surface of the airfoil increases in the gap and flows to two places, respectively. Part of the airflow accelerates from the gap between the tail of the slat and the leading edge of the main wing, flows backwards with the airflow on the upper surface of the airfoil, and accelerates the flow to the convergence of the upper surface of the main wing. Moreover, the velocity of airflow in the boundary layer on the upper surface of the wing is increased to eliminate a large number of vortices [7]; the other part flows to the cavity of the concave pressure surface of the slat, forming a recirculation zone. The velocities of these two streams differ greatly; a strong free shear layer is, therefore, formed at the interface. This shear layer originates from the sharp lower trailing edge and develops downstream with the separation vortex. When the separation vortex hits the trailing edge wall of the slat, a part of the vortex will flow back into the concave cavity of the slat, interfering with the new shear layer near the lower trailing edge [8] and forming return feedback [9]. In order to improve the lift–drag characteristics, grid flow channels can be added to the slats to improve the flow field in the slats. Grid fins [10], as multi-surface control systems consisting of an external frame and an internal grid partition, originate from the lift device composed of multiple elements used in the early design of aircraft, and have the advantages of high control efficiency, a large stall angle of attack, small hinge torque, and easy folding. In particular, their lift characteristics are good, and it is not easy to stall the devices with a high angle of attack, meaning they maintain good linearity. However, due to the defects in the structure, weight, resistance and technology of multi-element lift devices under the technical conditions of the time, single-element lift devices have been dominant in aircraft design for a long time. With the development of technology, the performance characteristics of grid fins derived from multi-element lift devices are increasingly understood, and their advantages as aerodynamic stabilizing and controlling surfaces for various types of aircraft continue to be highlighted. Research from Russia, the United States, Germany, and China has strengthened the understanding of grid fins; as a result, theoretical and applied achievements have been realized [11–15].

Wang Long et al. [16] carried out a numerical simulation on four different slotting positions of wind turbine blades by means of a computational fluid dynamic method, and obtained the flow field and lift coefficient of the blades at different angles of attack. They found that, under high angles of attack, the jet formed by slots can effectively inhibit flow separation, and the aerodynamic performance was better when the slotting position was near the separation point. Hui Zenghong et al. [17] studied the aerodynamic characteristics of multi-element leading slat lift devices using the pressure measurement method and obtained a better leading slat scheme by comparing the influence of different configuration slats on the airfoil lift effect and aerodynamic efficiency. Zhang Lijun et al. [18] proposed a scheme of symmetrical slitting in the wind separation zone for the vertical axis wind wing NACA0012 studied, which delayed the separation of the airfoil boundary layer and improved the aerodynamic performance of the airfoil. Liu Zhongyuan et al. [19], taking the L1T2 three-element airfoil as the research object, proposed carrying out slot control on the leading-edge slat to slow down the boundary layer separation and reduce its impact on the wake. They focused on the slot location, the flow direction at the slot outlet, and the flow control technology in order to improve the stall characteristics of the lift enhancement device. Although there is a lot of research on the flow control of slats, most of this research focuses on the slot position and slot angle. There is relatively little optimization research on the slot layout scheme, slot width, and slot and chord angles of slotted airfoils of multi-element configuration, which limits the potential of the flow control effect of slats.

In this paper, a grid-slat flow control configuration is proposed to increase lift, reduce drag and suppress flow separation. The quadratic curve parametric modeling method is used for the slot, and the design of the experiment aims to optimize its design. The optimal design parameters of the grid-slat configuration under the given design space and flow conditions are determined through numerical simulation. Moreover, the flow control mechanism of the optimal configuration and the influence and correlation of each design parameter on the lift–drag coefficient are analyzed. It provides a new idea and method for the design of three-dimensional grid multi-element airfoil lift devices in the future.

2. Flow Control Optimization Strategy for Leading-Edge Slot of the Airfoil 30P30N Based on Grid Fin

The grid-slat configuration can improve the flow field level of the slot by increasing grid flow channels. Its basic principle is that, in addition to increasing the flow path of the leading-edge slats, the slats themselves generate additional lift. More importantly, a new additional slot is formed on the basis of the original single channel, which can enhance the flow characteristics of the original slot, improve its disturbance characteristics to the flow of the main wing, and thus enhance the flow control effect. However, since there are many design parameters involved due to the addition of slots in the slats, this paper constructs an aerodynamic optimization design method for grid-slat flow control based on the DOE algorithm.

2.1. Design of Grid Fin–Slat Composite Configuration

The grid-slat configuration is designed on the multi-section airfoil 30P30N of the high-lift device, and the configuration is parameterized to facilitate the transformation of the original optimization of the geometric model of the configuration into the optimization of the configuration design parameters.

Analytic geometric curves can be expressed using explicit functions with few design variables. For example, in the typical conic curve method, section control can be realized by the beginning and end coordinates of curves, as well as by the tangent slope and shape parameters. It has fewer control parameters, which is conducive to the optimal design of the aerodynamic shape. The general equation of a conic curve is: $y^2 + ax^2 + bxy + cx + dy + e = 0$. The conic curve can be regarded as a conic obtained by performing plane oblique cutting. By changing the angle of the tangent plane, conic curves such as circle, ellipse, parabola and hyperbola can be obtained [20].

The slot at the leading edge is separately described by two curve equations, as shown in Figure 1, curves 1-2-3 and 4-5-6, respectively. Assuming that point 2 is the origin of the curve coordinate system, where the slope of the curve is infinite, the 1-2-3 elliptic equation can be simplified as $y^2 + ax^2 + bxy + cx = 0$. Then, the equation can be obtained according to the coordinates and slope of the curve at point 1 and the tangent equation of the curve at point 3.

Among them, the designer gives the x coordinates of point 1, and the x and y coordinates of point 2. The method to determine the tangent equation at point 3 is shown in the figure above. First, a straight line should be made through the two points denoted as AB. The angle between AB and the horizontal direction is k_3; then, the distance of y_3 is offset upward, where k_3 and y_3 are also given by the designer. The curve 4-5-6 is determined in the same way with the parameters x_4, x_5, y_5 and k_6. In conclusion, the chord length direction is assumed to be the x axis and the direction perpendicular to the chord length is assumed to be the y axis. Considering the calculation time and cost as well as the configuration changes, the control variables of the slot at the leading edge are shown in Table 1:

Table 1. Design variable and value range.

Design Variable	x_1 **(mm)**	x_2 **(mm)**	y_2 **(mm)**	y_3 **(mm)**	k_3 **(°)**
value range	11 ± 30%	9 ± 15%	11 ± 15%	0–6	40 ± 15%
Design Variable	x_4 **(mm)**	x_5 **(mm)**	y_5 **(mm)**	y_6 **(mm)**	k_6 **(°)**
value range	16 ± 30%	9 ± 15%	11 ± 15%	0–6	35 ± 15%

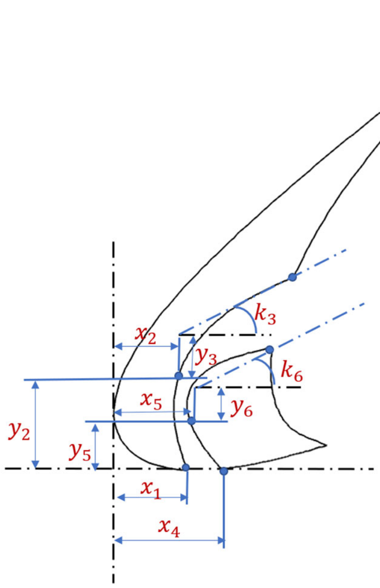

Figure 1. Grid-Slat configuration parameterization diagram.

The position and size of the slot inlet can be adjusted by adjusting x_5 and x_4 The degree of shrinkage can be adjusted by adjusting x_2 and x_5. Adjusting y_2 and y_5 can change the longitudinal position of the transition between the contraction and expansion of the joint. The position of the slot outlet position can be adjusted by adjusting x_3 and x_6. The shape of the expansion segment can be controlled by adjusting k_3, y_3, k_6 and y_6.

2.2. Aerodynamic Optimization Model of Grid-Slat Composite Configuration

The DOE module in the Isight-integrated platform is adopted, and the numerical optimization of control design parameters is used to replace the optimization of grid-slat configuration geometry. It is a structured research method used to systematically study the relationship between the independent variable and the dependent variable. This method studies the effect of one or more input parameters (factors) on multiple output results (responses) by arranging experiments scientifically and reasonably and replacing comprehensive tests with partial tests. The seven steps of the DOE experiment design are target determination, process analysis, factor screening, fast approach, factorial experiment, regression experiment, and robust design. The optimized design variables are parameters in the parameterized expression of grid-slat curve configuration $(x_1, x_2, y_2, y_3, k_3, x_4, x_5, y_5, y_6, k_6)$. The objective of optimization is to obtain the maximum lift–drag ratio K. The calculation formula is as follows:

$$C_l = \frac{L}{0.5\rho U_\infty^2 c} \tag{1}$$

$$C_d = \frac{D}{0.5\rho U_\infty^2 c} \tag{2}$$

$$K = C_l / C_d \tag{3}$$

As shown in Figure 2, the optimization process of grid-slat configuration is as follows:

(1) The optimization module assigns values to ten design variables for the first time according to the constraints, and Catia establishes a two-dimensional parametric model of grid-slat configuration according to the assignment;
(2) The pointwise divides the structural grid and output of the case file for Fluent calculation;
(3) The flow field of the grid-slat configuration is calculated at an angle of attack of 16.3°, and outputs the corresponding lift coefficient C_l and drag coefficient C_d;
(4) The Calculator module feeds back the lift–drag ratio K into the optimization platform according to the formula;
(5) The DOE algorithm reassigns design variables according to the calculation results, and then enters the next round of optimization calculations.

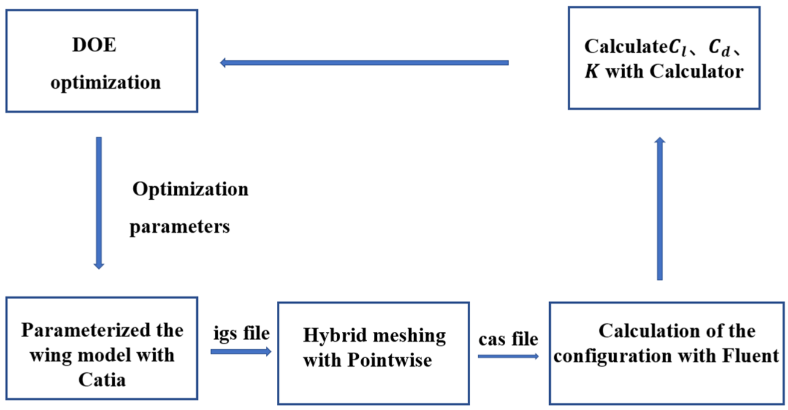

Figure 2. Optimization flow chart of grid-slat configuration.

3. Verification

3.1. Calculation Method and Verification of Aerodynamic Characteristics of the Multi-Section Airfoil 30P30N

In the present simulation, the flow field was assumed to be described by the 2D Reynolds-averaged Navier–Stokes (RANS) equations. The turbulence model adopted was the $k-\omega$ SST model. This turbulence model uses the damping function in the vortex viscosity model. It is more accurate at simulating the aerodynamic characteristics and pressure distribution of multi-section airfoil [21,22]. This has wide applicability and good prediction performance for separation flows with high-lift configurations.

The $k-\omega\ SST$ model formula is given as:

$$\begin{aligned} &\mu_t = \frac{\rho a_1 k}{\max(a_1\omega;\Omega F_2)} \\ &\frac{\partial(\rho k)}{\partial t} + u_i\frac{\partial(\rho k)}{\partial x_i} = P_k - \beta_k\rho k\omega + \frac{\partial}{\partial x_i}\left[\left(\mu_l + \frac{\mu_t}{\sigma_k}\right)\frac{\partial k}{\partial x_i}\right] \\ &\frac{\partial(\rho\omega)}{\partial t} + u_i\frac{\partial(\rho\omega)}{\partial x_i} = C_\omega P_\omega - \beta_\omega\rho\omega^2 + \frac{\partial}{\partial x_i}\left[\left(\mu_l + \frac{\mu_t}{\sigma_\omega}\right)\frac{\partial\omega}{\partial x_i}\right] + 2\rho(1-F_1)\frac{1}{\sigma_{\omega 2}}\frac{1}{\omega}\frac{\partial k}{\partial x_i}\frac{\partial\omega}{\partial x_i} \end{aligned} \quad (4)$$

The modified $k-\omega$ SST turbulence model constructs the model coefficient in the vortex viscosity coefficient of the equation as the following equation:

$$\alpha^* = \alpha^*_\infty\left[\frac{\alpha^*_0 + \frac{\mathrm{Re}_t}{R_k}}{1 + \frac{\mathrm{Re}_t}{R_k}}\right] \quad (5)$$

where $\mathrm{Re}_t = \rho\kappa/\mu\omega$ is the turbulent Reynolds number.

A numerical simulation of the 30P30N airfoil is taken as an example to verify the numerical simulation method of the two-dimensional lifting device adopted in this paper. The multi-section airfoil 30P30N of the high-lift device is widely used by CFD workers [23,24]. The deflection angle of the leading-edge slat and trailing-edge flap of this airfoil is 30°, the slot width of the leading-edge slat is 2.95%, and the overhang is −2.5%. The trailing-edge flap slot width is 1.27%, and the extension is 0.25% [23], as shown in Figure 3.

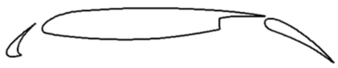

Figure 3. Geometry profile of 30P30N.

The comparative test data are the wind tunnel test results of McDonnell Douglas Aerospace and NASA Langley [25,26]. According to actual wind tunnel test conditions, the attack angles of the incoming flow are $-0.17^{\circ} \sim 21^{\circ}$. The Reynolds number is 9×10^6. The Mach number is 0.2. All the calculations provided here were obtained using the coupled solver of Fluent code. A second-order upwind difference scheme was chosen for momentum and turbulent kinetic energy, respectively. The incoming flow pressure is the standard atmospheric pressure. The mesh is generated as shown in Figure 4. For the component grid, we used a hybrid mesh with 40,792 cells. Wall spacing of the first layer is 1.71×10^{-3}, which satisfies $y+ \leq 1$.

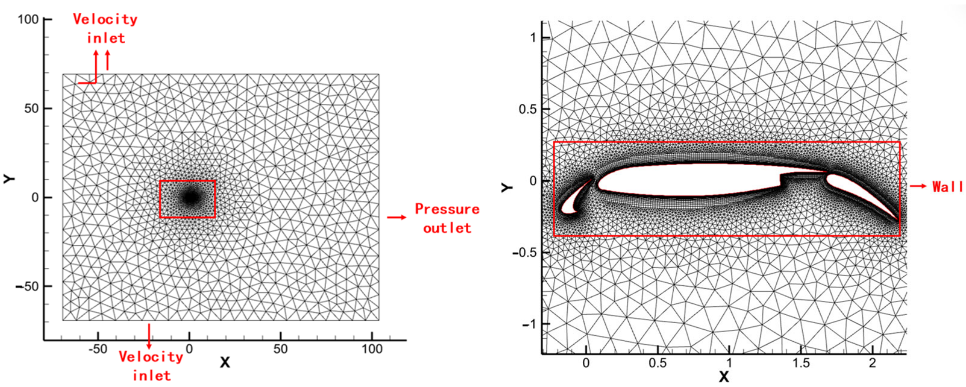

Figure 4. Computational mesh.

In the process of calculation, we monitored the convergence of residuals on the one hand, and found that the energy item decreases to 10^{-9} and other residuals except the energy item decrease to 10^{-4}. On the other hand, the calculation results cl or cd basically do not change with the increase in iteration steps. In Figure 5a, it seems that good agreement is achieved by comparing the calculated lift coefficient of the airfoil with the wind tunnel test results and that the deviation is large only near the stall angle of attack. As shown in Figure 5c,d, the surface pressure coefficients distribution of the main wing and flap coincide very well, and the pressure coefficients of the slats are basically consistent with the experimental data.

3.2. Grid Independence Verification

In order to ensure the accuracy of numerical calculation and reduce the calculation cost, the multi-section airfoil 30P30N is taken as an example to verify the independence of the computational grid. Three-grid generation schemes are used for simulation calculation. Table 2 shows the grid convergence verification results at an attack of 8°. The lift coefficient *Cl* converges with the increase in the number of grid cells. The drag coefficients, shown in Figure 6a, are basically the same using 2- and 3-grid generation schemes at different angles of attack. As shown in Figure 6c,d, the surface pressure coefficient distribution of the main wing and flap coincide very well. Using 2- and 3-grid generation schemes, the calculation results are similar, which meets the requirements of grid independence. Therefore, the grid division scheme of Case2 is adopted for subsequent calculations of cost.

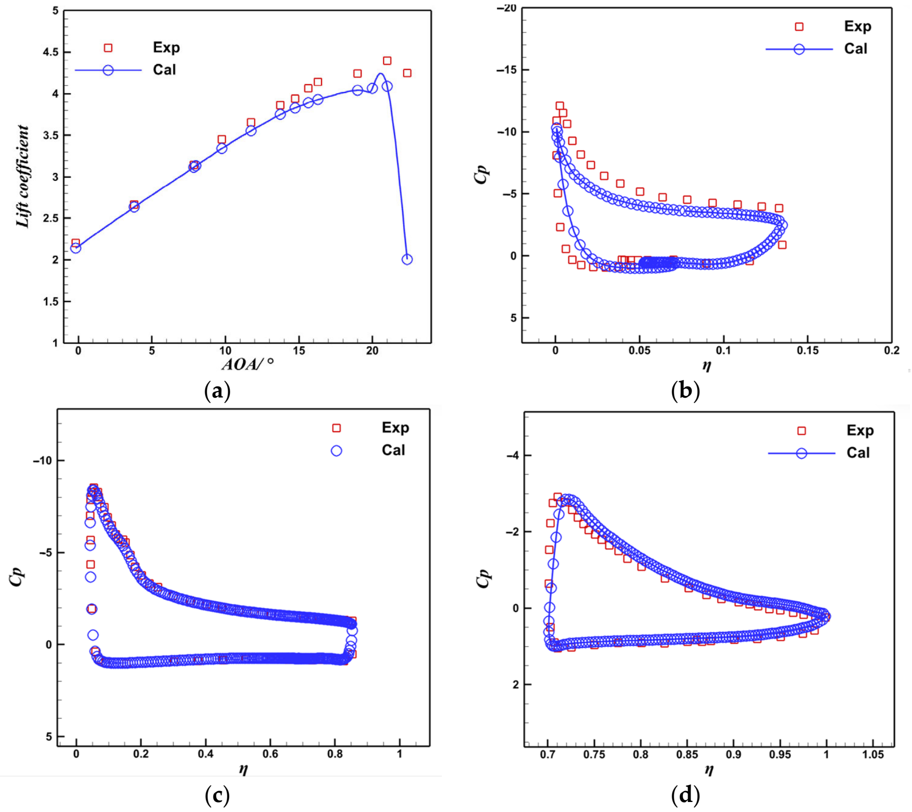

Figure 5. Verification results of 30P30N airfoil. (**a**) Lift Coefficient; (**b**) Slat Pressure Distribution [18,19]; (**c**) Main Pressure Distribution; (**d**) Flap Pressure Distribution.

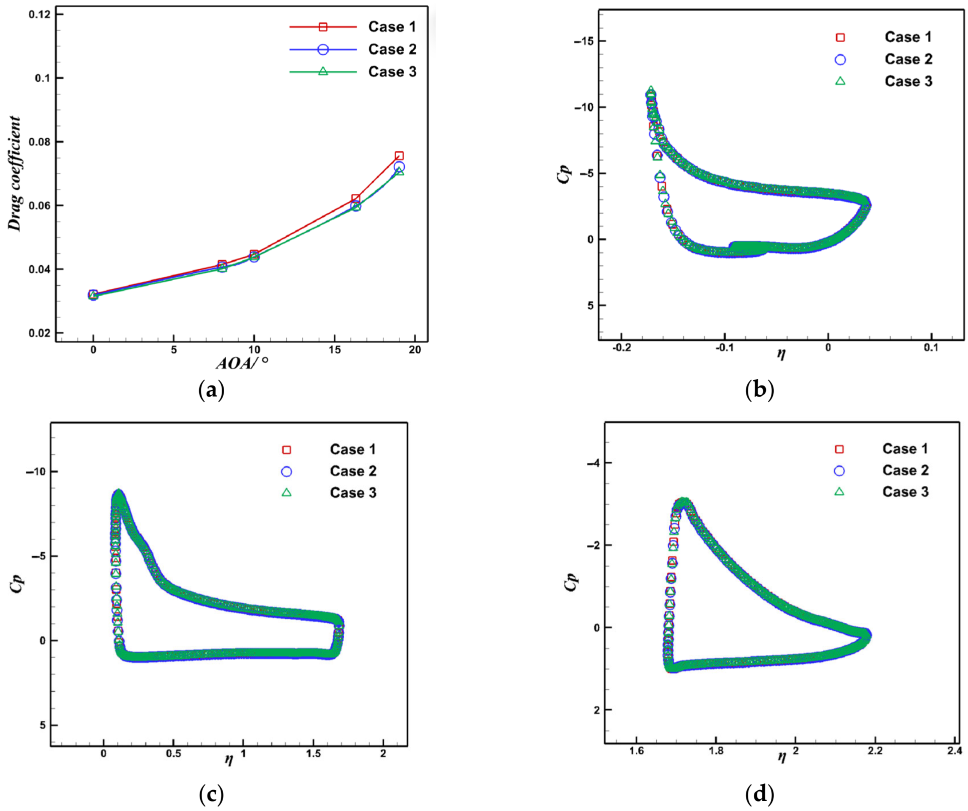

Figure 6. Grid independence verification. (**a**) Drag Coefficient; (**b**) Slat Pressure Distribution; (**c**) Main Pressure Distribution; (**d**) Flap Pressure Distribution.

Table 2. Grid independence verification.

Case	Grid Cell	Lift Coefficient
Case1	28,947	3.14498
Case2	40,792	3.13469
Case3	61,923	3.144985

4. Optimization Example and Analysis

Through optimization design, the values of design variables are shown in Table 3, and the configuration at this time is shown in Figure 7a. The grid-slat configuration plays a role in increasing lift and reducing drag through calculations. Figure 7b–d show the comparison of the lift coefficient, drag coefficient and lift–drag ratio between the original airfoil and the new configuration at different angles of attack. The simulation and optimization results show that the lift coefficient increases by 3.3%, the drag coefficient decreases by 12.7%, and the lift–drag ratio increases by 18.4% of the optimal configuration compared with the original airfoil at an angle of attack of 16.3°.

Table 3. Value of design variable.

Design Variable	x_1 **(mm)**	x_2 **(mm)**	y_2 **(mm)**	y_3 **(mm)**	k_3 **(°)**
optimal value	11	9	11	0	45
Design Variable	x_4 **(mm)**	x_5 **(mm)**	y_5 **(mm)**	y_6 **(mm)**	k_6 **(°)**
optimal value	16	11	11	0	30

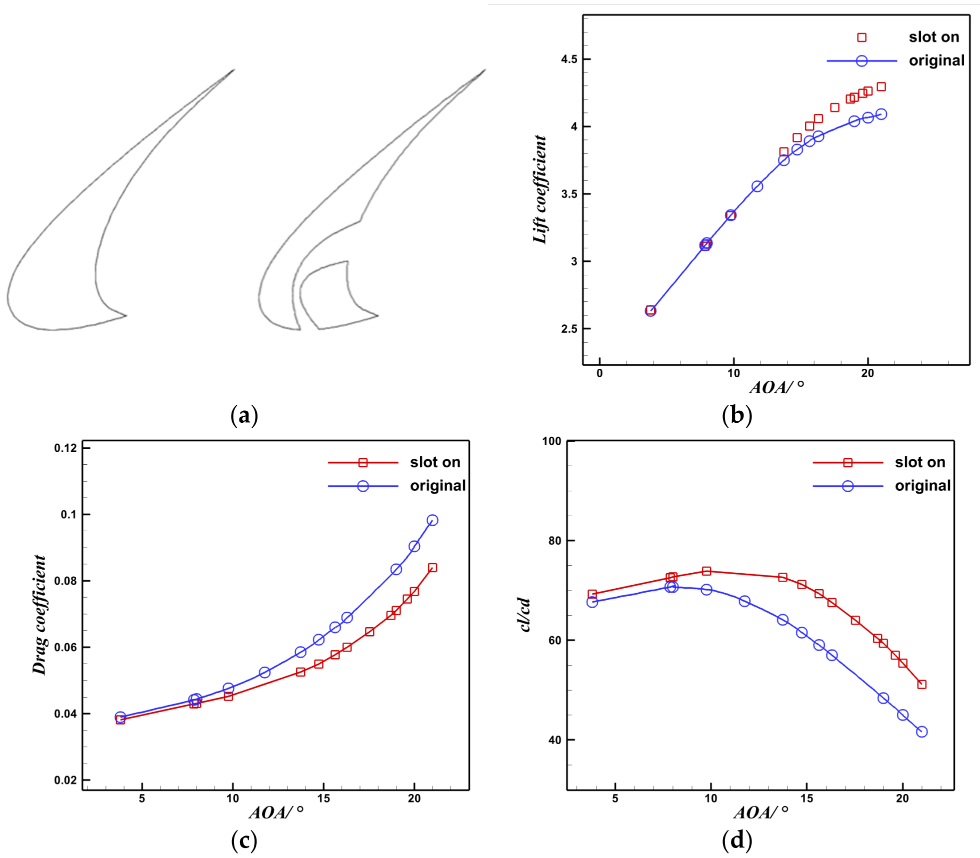

Figure 7. Numerical simulation comparison between original airfoil and optimal configuration. (**a**) Lift coefficient of slat; (**b**) Total lift coefficient; (**c**) Drag Coefficient; (**d**) Lift-drag ratio.

In order to further clarify the mechanism of increasing lift and reducing drag of grid-slat configuration, Figure 8 describes the total lift coefficients of the original airfoil and the optimized airfoil at different angles of attack. The lift coefficients, extracted separately from the slats, show that the configuration not only improves the lift of the slat itself but also improves the lift of the main wing.

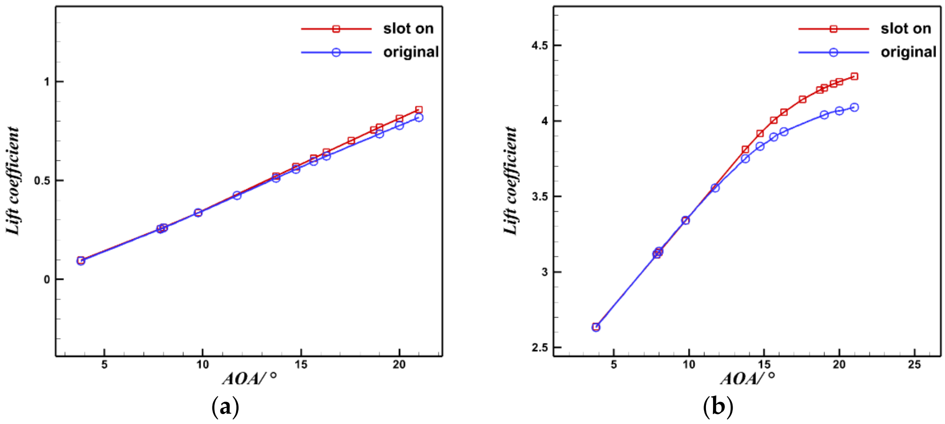

Figure 8. Comparisons of lift coefficients between original airfoil and optimal configuration. (**a**) Lift coefficient of slat; (**b**) Total lift coefficient.

The simulation results of the original airfoil and the optimized configuration at four typical angles of attack ($\alpha = 8°, 16.3°, 19°, 22.36°$) are compared and analyzed. The development process of wake flow is shown in Figure 9. For the original airfoil at an angle of attack of 22.36°, the wake flow area generated by the separation bubble is strongly mixed with the slot jet and the boundary layer of the main wing section, so that the rear section of the main airfoil and trailing-edge flap are in the mixed wake flow area. After optimization, the separation of grid-slat configuration is weakened, and the wake area is greatly reduced.

Superimposed contour plots of velocity magnitude and instantaneous streamlines at different angles are shown in Figure 10. Although the jet velocity has not yet reached the peak value, the velocities near the upper trailing edge are improved to varying degrees. The downstream flow-separated area near the upper trailing edge becomes a flow-attached area.

Figure 11 shows the surface pressure coefficient Cp of the original airfoil and the optimized layout under two operating conditions. For the convenience of differentiation, blue represents the original airfoil and red represents the optimal grid-slat configuration. The negative pressure value in the figure represents the suction on the upper surface of the wing. The positive pressure value represents the pressure on the lower surface of the wing. The pressure surface curve is located below the suction surface curve, indicating that the pressure on the lower surface is greater than that on the upper surface, which means the lift of the airfoil is positive [27,28]. The area enclosed by the pressure coefficient curve can roughly reflect the lift coefficient.

As is shown in Figure 11a, at an angle of attack of 19°, each suction peak of optimized configuration for each wing is slightly higher than that of the original wing, while the pressure surface curve is basically the same, so the optimal grid-slat configuration has a higher lift. As can be seen in Figure 11b, the suction peak of the original airfoil decreases sharply, and the area enclosed by the pressure coefficient curve decreases. However, the pressure coefficient curve of the optimized configuration is significantly different from that of the original airfoil, indicating that stall status had not been reached. Therefore, it can be concluded that the optimized configuration improves the aerodynamic characteristics at a high angle of attack and additionally increases the stall angle of attack.

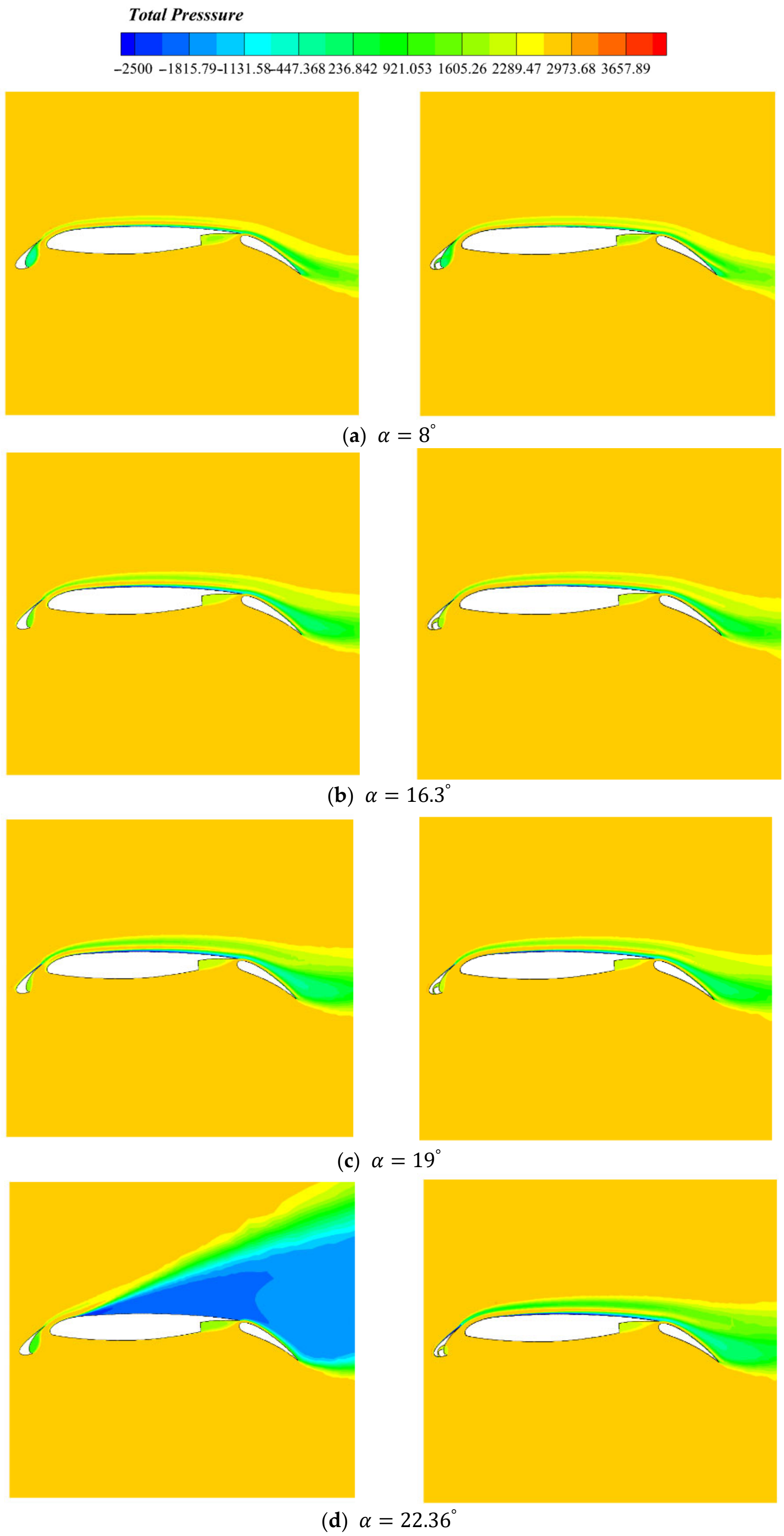

Figure 9. Comparison of wake flow development of the original airfoil and optimal grid-slat configuration.

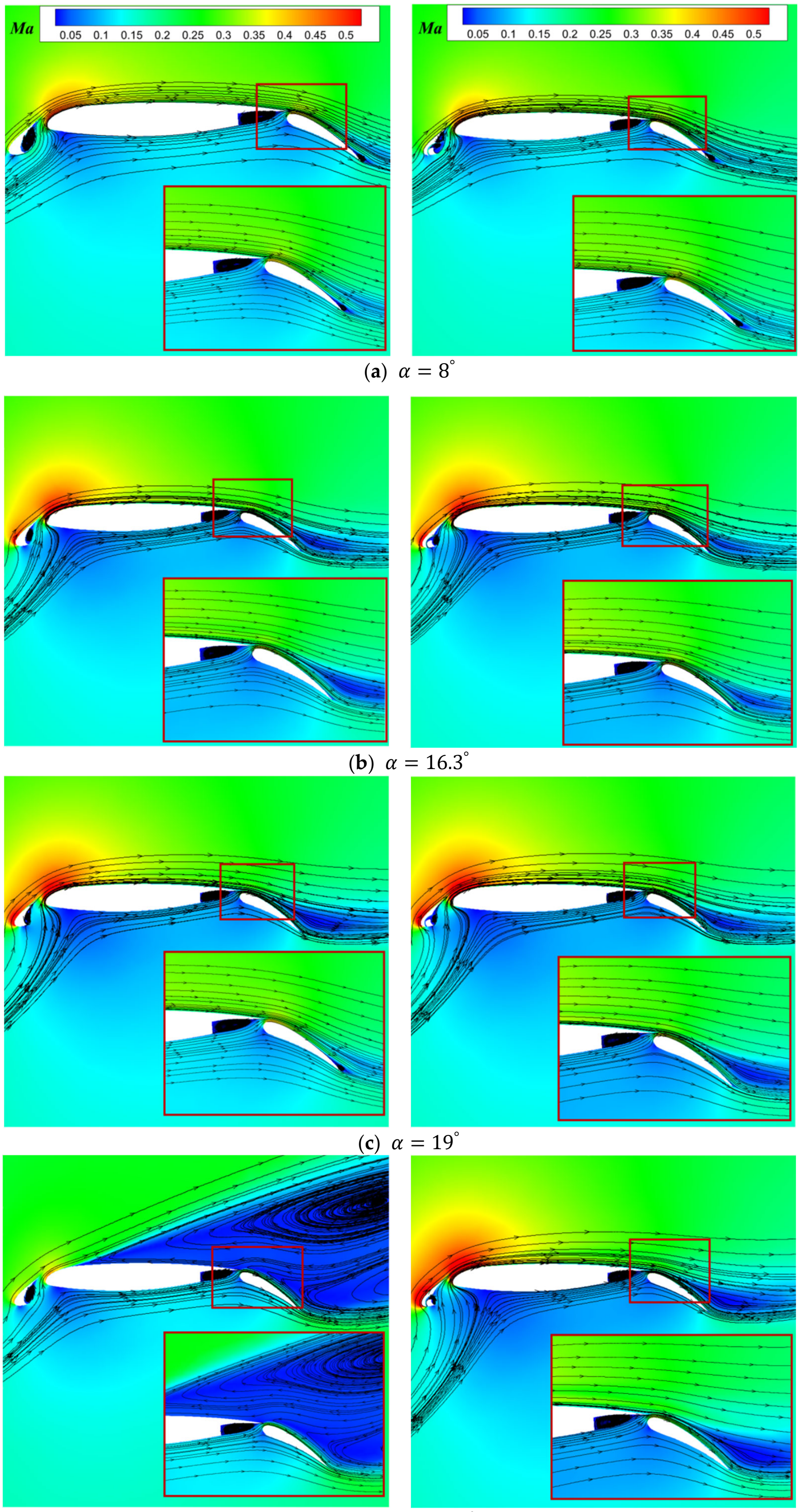

(**a**) $\alpha = 8^{\circ}$

(**b**) $\alpha = 16.3^{\circ}$

(**c**) $\alpha = 19^{\circ}$

(**d**) $\alpha = 22.36^{\circ}$

Figure 10. Contour comparison of the original airfoil and optimal grid-slat configuration at different attack angles.

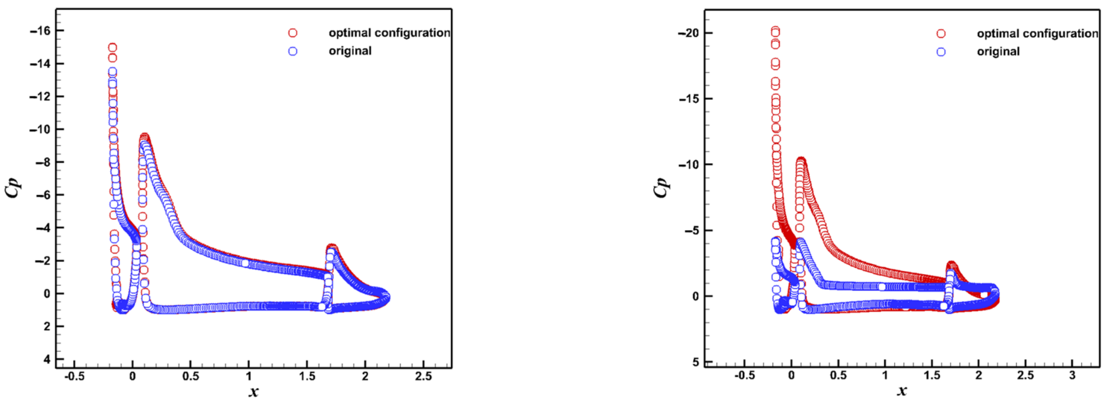

(**a**) α = 16.3° (**b**) α = 22.36°

Figure 11. Comparison of pressure coefficient between the original airfoil and optimal grid-slat configuration at different attack angle.

5. Influence Analysis of Design Parameters

In order to further clarify the design method of grid-slat configuration, the influence of each parameter on lift–drag coefficient and lift–drag ratio is analyzed according to the calculation results under the different design parameters calculated in the optimization process. First, the Pearson correlation coefficient [29] is selected to calculate and analyze the correlation between design parameters, lift–drag coefficient and lift–drag ratio, as shown in Table 4. The results show that the five design parameters are significantly related to the lift–drag ratio K, where x_1, k_3, k_6 are positively correlated with K, y_3, y_6 are negatively correlated with K.

Table 4. The correlation analysis results between design parameters and lift–drag coefficient.

		x_1	x_2	y_2	y_3	k_3
Cl	Pearson correlation	0.036	−0.048	−0.097	−0.164 **	123 *
	Sig. (2-tailed)	0.500	0.373	0.070	0.002	0.021
Cd	Pearson correlation	−0.113 *	0.010	−0.028	0.260 **	−0.277 **
	Sig. (2-tailed)	0.034	0.857	0.607	0.000	0.000
K	Pearson correlation	0.112 *	−0.019	0.004	−0.300 **	0.305 **
	Sig. (2-tailed)	0.036	0.720	0.948	0.000	0.000
		x_4	x_5	y_5	y_6	k_6
Cl	Pearson correlation	0.063	0.109 *	0.174 **	−0.123 *	0.287 **
	Sig. (2-tailed)	0.241	0.041	0.001	0.021	0.000
Cd	Pearson correlation	0.007	0.082	−0.017	0.279 **	−0.240 **
	Sig. (2-tailed)	0.902	0.123	0.747	0.000	0.000
K	Pearson correlation	0.000	−0.055	0.057	−0.308 **	0.311 **
	Sig. (2-tailed)	0.997	0.302	0.284	0.000	0.000

**. At 0.01 level (2-tailed), the correlation is significant. *. At 0.05 level (2-tailed), the correlation is significant.

Pearson's formula [30] is:

$$\rho_{X,Y} = \frac{\mathrm{cov}(X,Y)}{\sigma_X \sigma_Y} = \frac{E(XY) - E(X)E(Y)}{\sqrt{E(X^2) - (E(X))^2} - \sqrt{E(Y^2) - (E(Y))^2}} \tag{6}$$

where $\mathrm{cov}(X,Y)$ is the covariance of X and Y, and σ_X, σ_Y is the standard deviation of X and Y, respectively.

This shows that within the given range of variables, the shape of the slot changes with the change in five design parameters, which will greatly change the flow field. The change of x_1 results in the change of seam entry position, while the change of the other four design parameters y_3, y_6, k_3 and k_6 results in the change in seam shape. The design parameter x_1 is positively correlated, indicating that the lift force is better when the inlet position of the slot is closer to the right. The design parameters k_3 and k_6 are positively correlated, indicating that as the expansion degree of the slot increases, the acceleration degree of the slot to the flow is greater, and the lift force is better.

6. Conclusions

In this article, a flow control method of grid-slat configuration was proposed, and its optimal design was configured using the DOE algorithm. The optimal configuration was obtained and verified through numerical simulation, and we analyzed the flow control mechanism and the influence of design parameters. Two main conclusions were drawn from this study.

(1) By slitting the leading-edge slats, the lift–drag characteristics of the multi-element configuration can be effectively improved, which shows the feasibility and effectiveness of conducting flow control through the leading-edge slats. The simulation and optimization results show that the lift coefficient increases by 3.3%, the drag coefficient decreases by 12.7%, and the lift–drag ratio increases by 18.4% of the optimal configuration compared with the original airfoil at an angle of attack of 16.3°. The grid-slat can effectively improve the flow field level, and the flow always remains attached.

(2) The analysis of the correlation between the design parameters and the configuration of aerodynamic performance shows that the slot design parameters are highly sensitive to the final flow control effect, which also indicates that the flow control potential of the slats is very good.

In this paper, a flow control model and design optimization method based on slat slitting have only been constructed for a single grid slot. In future work, we expect to build a more effective slot scheme with the possibility of three-dimensional applications.

Author Contributions: Conceptualization, B.M.; Methodology, J.Y.; Writing—original draft, J.Y.; Writing—review & editing, B.M. All authors have read and agreed to the published version of the manuscript.

Funding: This research was funded by [National Natural Science Foundation of China] grant number [12202363] and [Natural Science Basic Research Program of Shaanxi] grant number [2021JQ-084].

Institutional Review Board Statement: Ethical review and approval were waived for this study because this article does not involve human or animal research.

Informed Consent Statement: Informed consent was obtained from all subjects involved in the study.

Data Availability Statement: The data is unavailable due to privacy.

Acknowledgments: The authors would like to acknowledge the support of National Natural Science Foundation of China (Grant No. 12202363) and the support of Natural Science Basic Research Program of Shaanxi (Program No. 2021JQ-084).

Conflicts of Interest: The authors declared no potential conflict of interest with respect to the research, authorship, and/or publication of this article.

References

1. Dam, C. The aerodynamic design of multi-element high-lift systems for transport airplanes. *Prog. Aerosp. Sci.* **2002**, *38*, 101–144.
2. Hammond, A.D. High-lift aerodynamics. In Proceedings of the Vehicle Technology for Civil Aviation, NASA SP-292, Hampton, VA, USA, 2–4 November 1971.
3. Shi, Q. Research on Flow Control of Wing for Increasing Lift and Reducing Drag. Ph.D. Thesis, National University of Defense Technology, Changsha, China, 2017.
4. Sun, R.M. Experimental Investigation on Aerodynamics Characteristics and Tip Vortices, of a Wing in Ground Effect. Ph.D. Thesis, Shanghai University, Shanghai, China, 2011.

5. Gross, J.; Traub, L.W. Experimental and Theoretical Investigation of Ground Effect at Low Reynolds Numbers. *J. Aircr.* **2015**, *49*, 576–586. [CrossRef]
6. Zhang, Q.Y.; Wang, Z.H.; Wei, M.; Lin, W. Review of high-lift devices design for amphibious aircraft. *Acta Aerodyn. Sin.* **2019**, *37*, 19–32.
7. Lin, Y.X. Design and Research of Flap Wing Sail for Wind-Assisted Vessel. Ph.D. Thesis, Dalian Maritime University, Dalian, China, 2013. (In Chinese)
8. Huang, H. Slat Noise Suppression with Upstream Mass Injection. Ph.D. Thesis, Shanghai Jiao Tong University, Shanghai, China, 2013. (In Chinese)
9. Sun, K.X. Study on Implicit Large Eddy Simulation Based on High-order Discontinuous Galerkin Method. Master's Thesis, Nanjing University of Aeronautics and Astronautics, Nanjing, China, 2019. (In Chinese)
10. Peng, K.; Hu, F.; Zhang, W.H.; Zhou, Z. Review of aerodynamic characteristics and application of grid fin. *J. Solid Rocket Technol.* **2015**, *38*, 8.
11. Washington, W.D.; Miller, M. S.0-I Experimental investigations of grid fin aerodynamics: A synopsis of nine wind tunnel and three flight tests. In Proceedings of the RTO AVT Symposium on Missile Aerodynamics, Sorrento, Italy, 11–14 May 1998.
12. Kretzschmar, R.W.; Burkhalter, J.E. 1-l Aerodynamic Prediction Methodology for Grid Fins. In Proceedings of the US Army Aviation and Missile Command, RTO Applied Vehicle Technology Panel Symposium, Sorrento, Italy, 11–14 May 1998.
13. Li, H.H.; Shi, Y.H. Current Status and Development Trend of Grid Fin. *Missile Space Vehcile* **2008**, *6*, 27. (In Chinese)
14. Fanucci, J.P.; King, M.J.; Gorman, J.J. Method for Producing Lattice Fin for Missiles or Other Fluid-Born Bodies. U.S. Patent No. 6,928,715, 16 August 2005.
15. Pruzan, D.A.; Mendenhall, M.R.; Rose, W.C.; Schuster, D. Grid Fin Stabilization of the Orion Launch Abort Vehicle. In Proceedings of the 29th AIAA Applied Aerodynamics Conference, Honolulu, HI, USA, 27–30 June 2011; American Institute of Aeronautics and Astronautics: Reston, VA, USA, 2011.
16. Wang, L.; Sun, L.; Zhang, J. Study of the impact of the change of slotted position at high angle of attack on wind turbine blades. *J. Hefei Univ. Technol. (Nat. Sci.)* **2017**. (In Chinese) [CrossRef]
17. Hui, Z.H.; Zhu, Z.X.; Zhang, L. Experimental investigation of aerodynamics performance of multi-element airfoil with leading-edge slat. *J. Exp. Fluid Mech.* **2007**, *21*, 17–20.
18. Zhang, L.J.; MA, D.C.; GU, J.W. Influence of shape of slotted airfoil on aerodynamic performance of vertical axis wind turbine. *J. Cent. South Univ. (Sci. Technol.)* **2019**. (In Chinese) [CrossRef]
19. Liu, Z.Y.; Chu, H.B.; Chen, Y.C.; Mao, J.; Zhang, B. Stall characteristics of high-lift device improved by slotting on leading-edge slat. *Acta Aerodyn. Sin.* **2022**, *40*, 21–28. (In Chinese) [CrossRef]
20. Dong, B.B. Design and Optimization of Two-Element Airfoil. Master's Thesis, Nanjing University of Aeronautics and Astronautics, Nanjing, China, 2012.
21. Halila, G.; Antunes, A.P.; Da Silva, R.; Azevedo, J.L.F. Effects of boundary layer transition on the aerodynamic analysis of high-lift systems. *Aerosp. Sci. Technol.* **2019**, *90*, 233–245. [CrossRef]
22. Zhang, Y.; Wang, S.; Sun, G.; Mao, J. Aerodynamic surrogate model based on deep long short-term memory network: An application on high-lift device control. *Proc. Inst. Mech. Eng. Part G J. Aerosp. Eng.* **2022**, *236*, 1081–1097. [CrossRef]
23. Wang, Y.T.; Wang, G.X.; Zhang, Y.L. Numerical study of complex flow over 30P-30N multi-element. *Acta Aerodyn. Sin.* **2010**, *28*, 5. (In Chinese)
24. Qin, P.G.; Liu, P.Q.; Qu, Q.L.; Peng, G. Influence of gap parameters on aerodynamics of multi-element airfoil. *J. Beijing Univ. Aeronaut. Astronaut.* **2011**, *37*, 4.
25. Valarezo, W.O.; Dominik, C.J.; Mcghee, R.J.; Goodman, W.L.; Paschal, K.B. Multi-Element Airfoil Optimization for Maximum Lift at High Reynolds Numbers. Available online: https://arc.aiaa.org/doi/10.2514/6.1991-3332 (accessed on 29 December 2022).
26. Chin, V.D.; Peters, D.W.; Spaid, F.W.; McGhee, R. Flowfield measurements about a multi-element airfoil at high Reynolds numbers. In Proceedings of the 23rd Fluid Dynamics, Plasmadynamics, and Lasers Conference, Orlando, FL, USA, 6–9 July 1993.
27. AI, G.Y. Numerical Simulation of Separated Flows around Isolated Airfoil at Different Reynolds Numbers. Master's Thesis, Chongqing University, Chongqing, China, 2017.
28. Cai, C.; Zuo, Z.G.; Liu, S.H.; Wang, X.; Wu, Y.L. Numerical Analysis on the Influence of Wavy Leading Edge on Stall Characteristics of a Wind Turbine Airfoil. *J. Eng. Thermophys.* **2015**, *3*, 531–534. (In Chinese)
29. Jin, L.; Li, Y. Discrimination of several correlation coefficients and their implementation in R software. *Stat. Inf. Forum* **2019**, *34*, 3–11. (In Chinese)
30. Xiao, X.; Jiang, B.; Ren, Q.; Yin, X.; Lu, J. Photovoltaic data cleaning based on interpolation and Pearson correlation. *Inf. Technol.* **2019**, *5*, 19–22. (In Chinese)